Rectifying Proposal Failures in Metropolis Light Transport

ANONYMOUS AUTHOR(S)
SUBMISSION ID: PAPERS_134

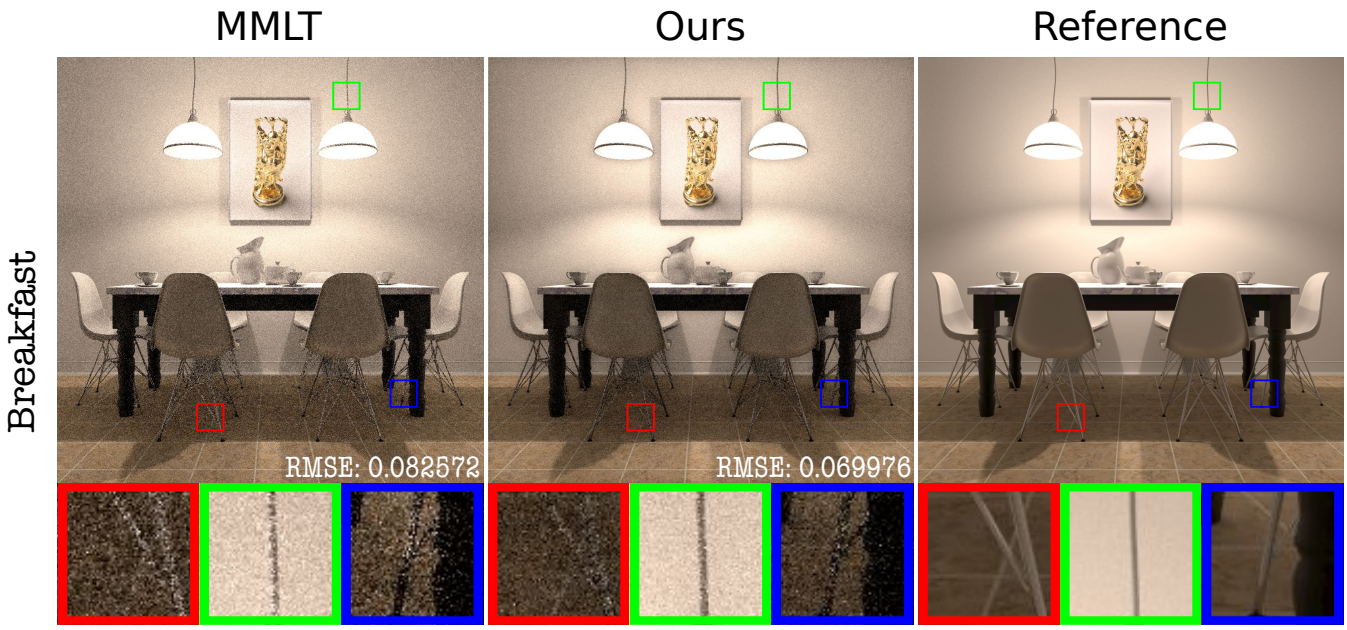

Fig. 1. *The Breakfast scene.* Equal-time comparison. Left: Image rendered with MMLT, where more than 37% of the traced paths are proposal failure paths. Middle: Excluding proposal failure paths from the states of Markov chain, our method produces higher quality results with the same computation. If our method is used to produce the same RMSE/quality result as MMLT does, in general, about a third of the computation will be saved.

Metropolis light transport (MLT) rendering algorithms rely on path mutations to explore the sample spaces. Mutated paths that carry zero radiance, such as those blocked by scene geometry, can significantly slow down the convergence of these algorithms. We call such zero-contribution paths *proposal failures*. We present a simple modification of MLT, Rectified Proposal Failure MLT (PFMLT), which excludes path duplications caused by proposal failures. PFMLT better approximates the original path distributions especially for high proposal rejection rates, and can be easily integrated with various MLT algorithms. We analyze our method with numerical models, and demonstrate better quality/performance trade-offs than Multiplexed MLT (MMLT) and Reversible Jump MLT (RJMLT) with various scenes of challenging lighting, geometry, and material conditions.

CCS Concepts: • **Mathematics of computing** → *Metropolis-Hastings algorithm*; • **Computing methodologies** → *Ray tracing*.

Additional Key Words and Phrases: Monte Carlo, rendering, sampling

0730-0301/2019/7-ART1 $15.00
https://doi.org/

ACM Reference Format:
Anonymous Author(s). 2019. Rectifying Proposal Failures in Metropolis Light Transport. *ACM Trans. Graph.* 1, 1, Article 1 (July 2019), 11 pages.

1 INTRODUCTION

Physically-based rendering is widely used to produce realistic images, but solving the rendering equation [Kajiya 1986] remains challenging, especially for scenes with complex lighting, geometry, or material. Metropolis Light Transport (MLT) algorithms can efficiently explore such challenging scenes by path mutations [Bitterli et al. 2018; Hachisuka et al. 2014; Hanika et al. 2015; Jakob and Marschner 2012; Kelemen et al. 2002; Li et al. 2015; Otsu et al. 2018, 2017; Pantaleoni 2017; Veach 1997]. However, the percentage of zero-radiance paths, which we call *proposal failures*, in those algorithms can be high and thus slow down the rate of convergence.

To address this issue, we propose Rectified Proposal Failure MLT (PFMLT), which distinguishes proposal failure paths from normal proposed paths and excludes them from the states of Markov chain. Our method can provide better quality/performance trade-offs (Figure 1), is simple to implement, and can be integrated with various MLT algorithms. We provide analysis, examples, and comparisons with Multiplexed MLT (MMLT) [Hachisuka et al. 2014] and Reversible Jump MLT (RJMLT) [Bitterli et al. 2018].

2 RELATED WORK

Light Transport Simulation. Light transport equation was first described by [Kajiya 1986]. [Veach 1997] presented that light transport simulation can be expressed as the integral:

$$I_j = \int_\Omega h_j(\bar{x}) f(\bar{x}) d\mu(\bar{x}) \tag{1}$$

, where I_j is the intensity of the j-th pixel of image, $\Omega = \bigcup_{k=1}^{\infty} \Omega_k$ is the space of light paths of all finite lengths k, $\bar{x}$ is a light path, $h_j()$ is the reconstruction filter that selects out all the light paths that contribute to the j-th pixel, f is the contribution of $\bar{x}$ and μ is the area measure.

Monte Carlo Integration. The integral in Equation (1) is infinite-dimensional because of the length of $\bar{x}$ can be infinite, which cannot be solved analytically. Monte Carlo numerical integration methods provide one solution to this kind of problem. The Monte Carlo integration estimator of Equation (1) is:

$$I_j \approx \hat{I}_j = \frac{1}{N} \sum_{i=1}^{N} \frac{h_j(\bar{x}^{(i)}) f(\bar{x}^{(i)})}{p(\bar{x}^{(i)})} \tag{2}$$

, where $\bar{x}^{(i)}$ is the i-th independently sampled light path, $p(\bar{x}^{(i)})$ is the probability density of the sample and N is the total number of samples.

In order to decrease the variance of the estimator, $p(\bar{x}^{(i)})$ should be approximately proportional to $f(\bar{x}^{(i)})$. Unfortunately, $f(\bar{x}^{(i)})$ is a spectrally valued function, and thus there is no unambiguous notion of what it means to generate samples proportional to $f(\bar{x}^{(i)})$. To address this issue, a scalar contribution function f^* is defined as the luminance of the path contribution f. Intuitively, $p(\bar{x}^{(i)})$ can be $f^*(\bar{x}^{(i)})/b$ (where b is the normalization constant $\int_\Omega f(\bar{x}) d\mu(\bar{x})$). So, Equation (2) can be presented as:

$$I_j \approx \hat{I}_j = \frac{b}{N} \sum_{i=1}^{N} \frac{h_j(\bar{x}^{(i)}) f(\bar{x}^{(i)})}{f^*(\bar{x}^{(i)})} \tag{3}$$

Now, we face two problems: calculating b and geting samples from $p(\bar{x}^{(i)})$ that is $f^*(\bar{x}^{(i)})/b$. The value b is typically estimated with another independent rendering algorithm such as bidirectional path tracing ([Lafortune and Willems 1993, 1996; Veach and Guibas 1994]). Then, the only problem is how to do the sampling.

Path-Space MLT.. The remaining problem in Equation (3) is how to get sample $\bar{x}^{(i)}$ in path space Ω with probability density $p(\bar{x}^{(i)})$ proportional to it's function value $f(\bar{x}^{(i)})$, which is so-called *importance sampling*. Veach[Veach and Guibas 1997] originally introduced Metropolis-Hastings (MH) sampling ([Hastings 1970; Metropolis et al. 1953]) into computer graphics and proposed a novel rendering algorithm, Metropolis Light Transport (MLT).

The mathematical foundation of MH sampling is building a Markov chain whose stationary distribution is exactly the target distribution. After reaching its stationary distribution, every subsequent mutation state of the Markov chain is a valid sample of the target distribution. However, it's never easy to know when the stationary is reached. MH sampling provides a practically way to solve this problem. It generates a set of samples from a non-negative function f that is distributed proportionally to $f's$ value without waiting for the stationary and whithout requiring the evaluation of b in two steps:

- *Proposal.* A new proposal path $\bar{y}$ is obtained from current path $\bar{x}$ by a mutation kernel $Q(\bar{y}|\bar{x})$.
- *Acceptance-Rejection.* Acceptance rate α is calculated:

$$\alpha(\bar{y}|\bar{x}) = \min\left(1, \frac{f^*(\bar{y})Q(\bar{x}|\bar{y})}{f^*(\bar{x})Q(\bar{y}|\bar{x})}\right) \tag{4}$$

  . Then accept the proposal path $\bar{y}$ with the probability α, otherwise reject it.

Mutation kernel Q is the key factor increasing acceptance rate and computation efficiency. In rendering algorithms, mutation kernel Q actually is the strategy to get proposal paths. The original MLT designs three mutation strategies targeting specific families of light paths, such as caustics or paths containing sequences of specular-diffuse-specular interactions. Some other mutation strategies have been developed in variants of path-space MLT, such as MEMLT [Jakob and Marschner 2012] for specular interactions, HSLT [Hanika et al. 2015] for rough materials, and GeoMLT [Otsu et al. 2018], which incorporates visibility into mutation strategies of MCMC rendering.

Primary Sample Space MLT.. Mutating in path space is not symmetric, which means that $Q(\bar{x}|\bar{y})$!= $Q(\bar{y}|\bar{x})$. This makes implementing these rendering algorithms a significant undertaking and makes debugging a notorious task. [Kelemen et al. 2002] presented a new MLT-type algorithm, Primary Sample Space MLT (PSSMLT), whose mutation strategy works in the unit cube of pseudo-random numbers, which is symmetric and easy to implement. The unit cube is called Primary Sample Space U.

PSSMLT converts random numbers $\bar{u}$ into light path $\bar{x}$ by path sampling. $\bar{x}$ can be thought of as being mapped from $\bar{u}$ by the inverse cumulative distribution function $P^{-1}(\bar{u})$, where $P(\bar{u}) = \int_0^{\bar{u}} p(\bar{u}')d\bar{u}'$. That is: $\bar{x} = P^{-1}(\bar{u})$. For the brevity of notation, we define:

$$\begin{aligned} C(\bar{x}) &= \frac{f(\bar{x})}{p(\bar{x})} \\ \hat{C}(\bar{u}) &= C(P^{-1}(\bar{u})) = C(\bar{x}) \\ \hat{p}(\bar{u}) &= p(P^{-1}(\bar{u})) = p(\bar{x}) \\ \hat{h}_j(\bar{u}) &= h_j(P^{-1}(\bar{u})) = h_j(\bar{x}) \end{aligned}$$

Then, in primary sample space, Equation (1) can be expressed as:

$$I_j = \int_U \hat{h}_j(\bar{u})\hat{C}(\bar{u}) d\bar{u} \tag{5}$$

Like Equation (3), the Monte Carlo integration estimator of Equation (5) can be presented as:

$$I_j \approx \hat{I}_j = \frac{b}{N} \sum_{i=1}^{N} \frac{\hat{h}_j(\bar{u}^{(i)})\hat{C}(\bar{u}^{(i)})}{\hat{C}^*(\bar{u}^{(i)})} \tag{6}$$

, where $\hat{C}^*$ is the luminance of the importance function $\hat{C}$. Mutating in primary sample space is symmetric. That is $Q(\bar{u}|\bar{v}) = Q(\bar{v}|\bar{u})$, which makes implementing PSSMLT much easier, and which also avoids the computation of the transition probabilities altogether. So,

the calculation of acceptance rate can be simplified as:

$$\alpha(\bar{v}|\bar{u}) = \min\left(1, \frac{\hat{C}^*(\bar{v})}{\hat{C}^*(\bar{u})}\right) \tag{7}$$

, where $\bar{v}$ is the proposal state of $\bar{u}$ in primary sample space.

PSSMLT makes the integrand much flatter, and increases the average acceptance rate and therefore reduces the variance. The generality of PSSMLT has led to a lot of applications, such as [Gruson et al. 2017; Hachisuka and Jensen 2011; Hoberock and Hart 2010; Kitaoka et al. 2009; Šik et al. 2016]. As mentioned before, the method of conversion from random numbers $\bar{u}$ into light path $\bar{x}$ is path sampling. Actually, PSSMLT adopts bidirectional path tracing to do the path sampling. Bidirectional path tracing produces many paths from a single primary sample by using different connection strategies to connect camera sub-path and light sub-path. And then, the connected path of maximum luminance is selected as the final proposal light path. Unfortunately, the process of finding the path of maximum luminance is not efficient.

Multiplexed MLT.. In order to solve the efficient problem of PSSMLT, [Hachisuka et al. 2014] presented an extension to PSSMLT called Multiplexed Metropolis Light Transport (MMLT) which combines MCMC algorithm with Multiple Importance Sampling [Veach 1997]. Instead of always implementing all BDPT connection strategies and finding the path of maximum luminance, the algorithm chooses a single strategy according to an extra random number and returns its contribution scaled by the inverse discrete probability of the choice. The additional random number used for strategy selection can be mutated in the same way as the other components of $\bar{u}$ in primary sample space. The Monte Carlo Integration estimator is generalized as:

$$I_j \approx \hat{I}_j = \sum_{t=1}^{M} \frac{b}{N_t} \sum_{i=1}^{N_t} \frac{\hat{h}_j(\bar{u}^{(i,t)})\hat{w}_t(\bar{u}^{(i,t)})\hat{C}(\bar{u}^{(i,t)})}{\hat{C}^*(\bar{u}^{(i,t)})} \tag{8}$$

, where, t is determined by the extra state dimension and is used to choose sample technique, and $\hat{w}_t$ is a weighting function for any given path. The extension of the extra state dimension for choosing sample technique results that every mutation may change both random numbers from $\bar{u}$ to $\bar{v}$ and sample technique from t to t'. So, based on Equation (7), the calculation of acceptance rate is generalized:

$$\alpha((\bar{v}, t')|(\bar{u}, t)) = \min\left(1, \frac{\hat{w}_{t'}(\bar{v})\hat{C}^*_{t'}(\bar{v})}{\hat{w}_t(\bar{u})\hat{C}^*_t(\bar{u})}\right) \tag{9}$$

This generalization produces the practical effect that the Metropolis sampler mainly focus on more effective strategies that leads to greater MIS-weighted contributions to the final image. Furthermore, the individual iterations of every Markov chain are much more efficient since they only execute a single connection strategy. Based on MMLT's approach, some developments have been made, such as H2MC[Li et al. 2015], which utilizes Hamiltonian Monte Carlo to adaptively control the shape of the transition kernels.

Bridging Path-Space and Primary-Sample-Space. In order to combine the flexibility of mutation strategies of path space MLT with the simplicity and efficiency of primary sample space MLT, several methods have been developed to bridge the two state spaces by using invertible mappings to transform samples between them, such as [Bitterli et al. 2018; Otsu et al. 2017; Pantaleoni 2017].

Analysis and Problem Statement. Generally, the improvements in MLT-type rendering algorithms can be classified into three categories. First, developments of mutation strategies in path space, such as MEMLT [Jakob and Marschner 2012] for specular interactions, HSLT [Hanika et al. 2015] for rough materials, and GeoMLT [Otsu et al. 2018], which incorporates visibility into mutation strategies. Second, developments of mutation strategies in primary sample space, such as MMLT and H2MC [Li et al. 2015]. Third, bridging the two spaces, so that the developments of mutation strategies in both spaces can be used in the same algorithm framework, such as [Bitterli et al. 2018; Otsu et al. 2017; Pantaleoni 2017].

All of these efforts are put on variant mutation strategies to increase the acceptance rate and to reduce the variance of their different aim scene scenarios. However, the ratio of proposal failures in traced paths is still a serious problem. For MMLT-related algorithms, things get worse, because they run many independent Markov chains with fixed depth of path for each chain, which increases the chance of confronting proposal failure paths.

Mathematically, given a constrained parameter space and an unconstrained Markov chain, proposal failures occur. With respect to this issue, [Robert 2013] presented that it is a correct method to subsample the chain and exclude proposal failures. Also, even though the method works as a low key accept-reject sampling, it may be more efficient than the original Metropolis-Hastings algorithm when the issue of proposal failures is serious. So, we introduce this idea into MLT and present a simple modification of MLT, Rectified Proposal Failure MLT (PFMLT), which excludes path duplications caused by proposal failures.

3 OVERVIEW

The main idea of our method is distinguishing proposal failure paths from normal proposal paths and then excluding them from the states of Markov chain, so that speed up the convergence rate of the Metropolis-Hastings sampler.

In Section 4, we propose Rectified Proposal Failure MCMC (PFMCMC), which simulates proposal failures by setting path radiance value to 0 with probability p_f and provides remedy for proposal failures. In Section 5, we combine PFMCMC with MMLT [Hachisuka et al. 2014] and RJMLT [Bitterli et al. 2018], and compare quality/performance with various scenes.

4 METHOD

Our algorithm, PFMCMC, restricts focus to the case of proposal failure. PFMCMC is an extension of Metropolis Hastings (MH) [Hastings 1970; Metropolis et al. 1953], one of the most popular, classical MCMC algorithms. PFMCMC is summarized in Algorithm 1. We aggregate some important terms of our notation in Table 1 for reference. From Algorithm 1, we can see that the basic structure of PFMCMC is similar to MH's. The major modification is that PFMCMC introduces probability p_f to simulate proposal failure shown the red part (line 4 to 7), and provides a remedy for the failure situation in the blue part (line 8 to 11).

Table 1. *Notations.*

Symbol	Meaning
X	Sample result set
X_0	Initial sample
X^*	Proposal sample
X_j	Current sample
X_{j+1}	Next sample
$f(X^*)$	Function value of proposal sample
$f(X_j)$	Function value of current sample
$sTotalNum$	Set # of total proposal
$rTotalNum$	Real # of total proposal
$TotalRep$	Total # of repetition for proposal failure
j	Proposal counter
p_f	Probability of proposal failure
α	Acceptance rate

Require: initial values X_0, $sTotalNum$, and failure possibility p_f.
Ensure: output sample set X

1: **for** $j \leftarrow 0; j < sTotalNum; j \leftarrow j + 1$ **do**
2: Draw a proposal value X^* from X_j
3: Calculate $f(X^*)$
4: Draw $v \sim U(0, 1)$.
5: **if** $v < p_f$ **then**
6: $f(X^*) \leftarrow 0$
7: **end if**
8: **if** $(f(X^*) = 0)$ **then**
9: $j \leftarrow j - 1$
10: **continue**
11: **end if**
12: Calculate acceptance rate α. $\alpha = \min\left(1, \frac{f(X^*)}{f(X_j)}\right)$
13: Draw $u \sim U(0, 1)$.
14: **if** $u < \alpha$ **then**
15: $X_{j+1} \leftarrow X^*$
16: **else**
17: $X_{j+1} \leftarrow X_j$
18: **end if**
19: **end for**
20: **return** X

Algorithm 1. *Rectified Proposal Failure MCMC (PFMCMC).* This is an extension of MH sampling, which simulates proposal failures by setting function value $f(X_j)$ to 0 with failure probability p_f (as shown in the red part) and gives a special remedy to proposal failures (as shown in blue part). Note that the red part is only for simulation (for methods with high p_f); the blue part can be applied to all MCMC-based algorithms with path multations.

Proposal Failure Simulation. $f(X_j)$ is the function of sample X_j. p_f indicates the overall probability of proposal's random failure. Generally, the percentage of zero-contribution paths in MMLT for our test scenes, like Figure 1, is between 35% and 65%. So we can set p_f at a value in $[0.35, 0.65]$ to verify the effectiveness of PFMCMC.

Proposal Failure Remedy. The basic idea of the remedy for proposal failures is excluding them from the states of Markov chain. To be specific, as shown in the blue part (line 8 to 11), the first step is detecting proposal failures, and the second step is shifting the sample counter j backward to exclude proposal failures. Here, we would like to highlight two things. First of all, the remedy does nothing to break the detailed balance, so our method is also unbiased. Then, the remedy has a positive effect—denoising, and a negative effect—under-sampling. In general, the effect of denoising surpasses the effect of under-sampling, so the net effect is a better approximation of the sample distribution, as exemplified in Figures 2 and 3.

4.1 Analysis

We illustrate the effect of PFMCMC with a 1D model based on a normal distribution function with a probability p_f of proposal failure. The effect comparison of PFMCMC and MCMC is based on equal sampling time. We use the total number of proposal $rTotalNum$ as an indicator of sampling overhead, which is more reliable because of the elimination of influences of system performance. For MCMC, $rTotalNum$ equals to $sTotalNum$. For PFMCMC, $rTotalNum$ is the additive result of $sTotalNum$ and $TotalRep$ which is related to p_f.

Parameter Setting. We are assuming that, for the normal distribution function, the mean is 3 and the standard deviation is 2. Considering that the percentage of proposal failure for most of scenes rendered with MMLT locates in the interval $[0.4, 0.6]$, we test two cases with p_f set at 0.4 and 0.6 respectively. For MCMC, $sTotalNum$ is set at 1600. For PFMCMC, in order to make $rTotalNum$ close at 1600, $sTotalNum$ setting is more complicate, which is affected by p_f: when p_f is 0.4, we set $sTotalNum$ at 960; when p_f is 0.6, we set $sTotalNum$ at 690.

Results Analysis. Figure 2 demonstrates the sample results of MCMC and PFMCMC. (a) and (c) show the results sampled with the extension of MCMC, which includes failure simulation and no remedy; (b) and (d) show the results sampled with the extension of MCMC, which is our PFMCMC including both failure simulation and remedy. We can see that PFMCMC gets better results than MCMC does.

	$p_f = 0.4$	$p_f = 0.6$
MCMC (reference)	$rTotalNum$: 1600 RMSE: 0.006834	$rTotalNum$: 1600 RMSE: 0.008760
PFMCMC, (similar $rTotalNum$)	$rTotalNum$: 1584 RMSE: 0.006370	$rTotalNum$: 1589 RMSE: 0.007728
PFMCMC, (similar RMSE)	$rTotalNum$: 1383 RMSE: 0.006787	$rTotalNum$: 1262 RMSE: 0.008686

Table 2. *Comparing MCMC with PFMCMC with average results of 100 runs each.* $rTotalNum$ controls cost. Lower RMSE value means higher quality.

Because of the use of correlated samples, a single run of an MCMC integrator may not be representative. We test every case for 100 times and average the corresponding results, which are recorded in Table 2. As shown, PFMCMC provides better quality/efficiency than MCMC under similar speed/quality.

As mentioned before, our method, exclusion of proposal failures, has a positive effect—denoising, and a negative effect—under-sampling. In general, the effect of denoising surpasses the effect

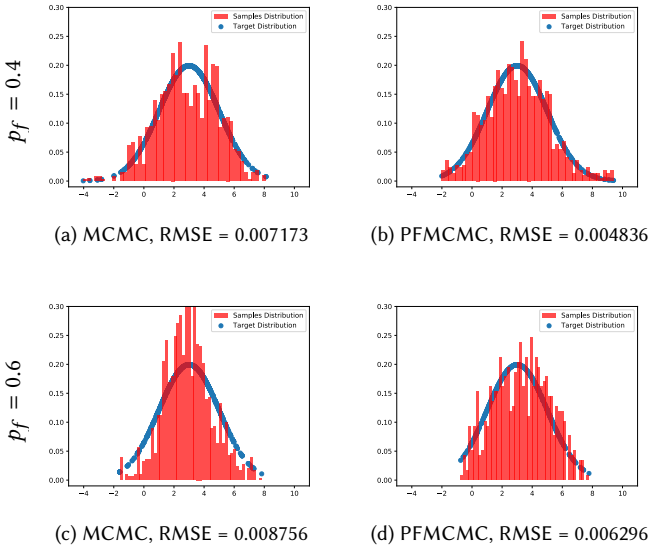

(a) MCMC, RMSE = 0.007173 (b) PFMCMC, RMSE = 0.004836

(c) MCMC, RMSE = 0.008756 (d) PFMCMC, RMSE = 0.006296

Fig. 2. *Sampling a 1D normal distribution under simulated proposal failures with MCMC and PFMCMC.* The total number of proposal is used as an indicator of sampling overhead. All of these results are produced with equal number of total proposals, 1600. The blue and red curves visualize the target and sample distributions. The top and bottom rows correspond to different p_f values, while the left and right column show results sampled with MCMC and PFMCMC. As expected, larger p_f triggers larger errors, but PFMCMC performs better than MCMC, as indicated by both the RMSE measurements and the visualized distributions.

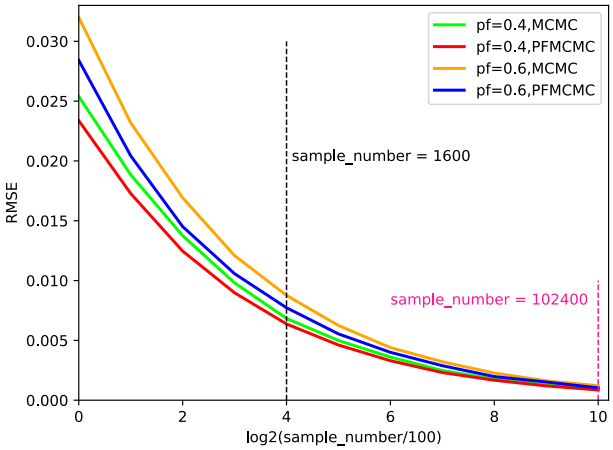

Fig. 3. *Convergence comparisons for sampling the 1D normal distribution with MCMC and PFMCMC.* For the four cases, "p_f=0.4, MCMC", "p_f=0.4, PFMCMC", "p_f=0.6, MCMC", "p_f=0.6, PFMCMC", we take 11 test points for each. And for each test point, we calculate its average result of 100 runs. From this plot, we can see: (1), As the number of samples increases, the advantage of our method decreases. For example, in the condition of a large number of samples, like 102400, our method produces almost the same results as MCMC does. (2), Our method shows less advantage in the case of lower rate of proposal failure. Fortunately, in practice, we rarely take extremely large number of samples and we frequently meet the case of high rate of proposal failure, so our method helps.

of under-sampling, so the net effect is a better approximation of the sample distribution. As the number of samples increases, both effects decrease. So, as shown in Figure 3, in the condition of a large number of samples, like 102400, our method just produces almost the same results as MCMC does. Also, our method shows less advantage in the case of lower rate of proposal failure. Fortunately, in practice, we rarely take extremely large number of samples, and our method can help cases of high rates of proposal failure.

5 IMPLEMENTATION

PFMCMC can be combined with different MLT-type algorithms with mutation in primary sample space or path space. An example demonstrated in this section is MMLT [Hachisuka et al. 2014]. MMLT improves rendering efficiency by selecting seed path with probability proportion to its contribution to the final image. Fusing MMLT with the idea of proposal failure remedy of PFMCMC makes PFMLT even much more efficient than MMLT. For example, rendering Breakfast scene in Figure 1 with PFMLT saves about 30 percent of the time to produce the same quality image as MMLT does. Algorithm 2 shows the pseudocode of PFMLT.

Initialization. First, the same as MMLT, we sample a seed path $\bar{s}$ from Initial Path Set and calculate it's depth k and contribution $f(\bar{x}_s)$. The depth k should be emphasized here, like MMLT, all of subsequent proposal paths are of the same depth as this seed path. Seed path $\bar{s}$ should be assigned to current path $\bar{x}$. $sTotalNum$ can be obtained by dividing total proposal number by total number of Markov chains. Then, some special variables for implementing the core idea of PFMCMC should be initiated. Proposal failure flag $IsFailure$ is initiated as 0.

Random Numbers Proposal. For MMLT, the same as PSSMLT, two main steps are needed to draw a proposal $\bar{y}$ from $\bar{x}$ in path space. Firstly, draw a proposal vector of random numbers $\bar{v}$ from $\bar{u}$ which is the primary sample space counterpart of $\bar{x}$. Secondly, obtain $\bar{y}$ by path sampling in path space using the proposal vector of random numbers $\bar{v}$. As to the first step, note that we apply normally distributed perturbations to each component of the vector of random numbers. The advantage of sampling with a normal distribution like this is that it naturally tries a variety of mutation sizes. It preferentially makes small mutations that remain close to the current state, which help locally explore the path space in small areas of high contribution.

Path Sampling and Potential Failures. As mentioned in "Random Numbers Proposal" part, the second step of path proposal is path sampling. It is this step where proposal failures occur. The proposal vector of random numbers $\bar{v}$ has four main uses in path sampling. First, one random number, v_s, of $\bar{v}$ is used to choose sample technique, so that t and s are determined. Second, a sub-vector, $\bar{v}_{camera}$, of $\bar{v}$, along with t, is used to sample a camera sub-path $\bar{y}_{camera}$ with depth exactly being t. Third, a sub-vector, $\bar{v}_{light}$, of $\bar{v}$, along with s,

Ensure: Accumulation of Path Contributions
1: Sample a seed path $\bar{s}$ from Initial Path Set
2: Calculate k (the depth of $\bar{s}$) and path contribution $f(\bar{x}_s)$
3: $\bar{s}$ is used as current path $\bar{x}$: $\bar{x} \leftarrow \bar{s}$, $f(\bar{x}) \leftarrow f(\bar{x}_s)$
4: $IsFailure \leftarrow 0$
5: **for** $j \leftarrow 0; j < sTotalNum; j \leftarrow j + 1$ **do**
6: Draw a proposal vector of random numbers $\bar{v}$ from $\bar{u}$.
7: $t \leftarrow \text{int}((k+2)v_s)$
8: $s \leftarrow (k+1) - t$
9: **if** $!(\bar{y}_{camera} \leftarrow \text{SampleCameraSubpath}(\bar{v}_{camera}, t))$ **then**
10: $IsFailure \leftarrow 1$
11: **end if**
12: **if** $!(IsFailure)$ **then**
13: **if** $!(\bar{y}_{light} \leftarrow \text{SampleLightSubpath}(\bar{v}_{light}, s))$ **then**
14: $IsFailure \leftarrow 1$
15: **end if**
16: **end if**
17: **if** $!(IsFailure)$ **then**
18: **if** $!(f(\bar{y}) \leftarrow \text{Connect}(\bar{y}_{camera}, \bar{y}_{light}, \bar{v}_{connect}))$ **then**
19: $IsFailure \leftarrow 1$
20: **end if**
21: **end if**
22: **if** $(IsFailure)$ **then**
23: $j \leftarrow j - 1$
24: $IsFailure \leftarrow 0$
25: **continue**
26: **end if**
27: $IsFailure \leftarrow 0$
28: Calculate acceptance rate α. $\alpha = \min\left(1, \frac{L(f(\bar{y}))}{L(f(\bar{x}))}\right)$
29: Draw $u \sim U(0,1)$.
30: **if** $u < \alpha$ **then**
31: $\bar{x} \leftarrow \bar{y}$
32: **end if**
33: AccumulatePathContribution$(f(\bar{x}))$
34: **end for**

Algorithm 2. *PFMLT (Rectified Proposal Failure MLT).* The blue part is the simple remedy for proposal failures. If proposal failure paths are detected, we exclude them from the states of Markov chain by shifting sample counter j backward before getting into the step of calculating acceptance rate.

is used to sample a light sub-path $\bar{y}_{light}$ with depth exactly being s. Fourth, a sub-vector, $\bar{v}_{connect}$, of $\bar{v}$ is used to connect $\bar{y}_{camera}$ and $\bar{y}_{light}$ to make a complete proposal path $\bar{y}$ and to calculate proposal path contribution $f(\bar{y})$.

Except for the first stage, the other three are of potential failures. In the sampling sub-path stages, the depth of camera sub-path $\bar{y}_{camera}$ may not be t, or the depth of light sub-path $\bar{y}_{light}$ may not be s, so failures happen. In the connecting stage, the connection between the two sub-paths, $\bar{y}_{camera}$ and $\bar{y}_{light}$, may be blocked, which is a very high probability event. The existence of these failures is the very reason why PFMLT is much more efficient than MMLT.

Failure Remedy. $IsFailure$ is used to indicate whether any failure has happened. If any failure is detected, the flag $IsFailure$ is set to 1. Note that if a failure has been detected earlier, the subsequent path sampling programs are not necessary to run.

If proposal failure paths are detected, we exclude them from the states of Markov chain by shifting sample counter j backward before getting into the step of calculating acceptance rate, which is shown in line 22 to line 26 of Algorithm 2.

Accept Probability. We used the same mutation function for getting the vector of random numbers $\bar{v}$ from $\bar{u}$ as MMLT. Since these mutations are all symmetric, transition probability density functions are not needed to evaluate, the acceptance probability α is simply the ratio of the luminosities of proposal path contribution $f(\bar{y})$ and current path contribution $f(\bar{x})$.

Contribution Accumulation. The same as MMLT, the scaling by the reciprocal of the discrete probability density of the selected path length as noted before, we also need to scale each contribution by the number of techniques $k+2$. This scaling corresponds to the fact that the chain explores $k+2$ different sub-spaces.

6 RESULTS

This section includes main results (Section 6.1) and extra results (Section 6.2). In Section 6.1, we implement our method by extending the system of PBRT, and we compare against MMLT implemented in the same system. In Section 6.2, we extend both RJMLT and MMLT in Tungsten [Bitterli 2017], a renderer that is a much simpler and faster than PBRT, and we compare against MMLT and RJMLT implemented in Tungsten.

6.1 Main Results

We implement our method by extending the system of PBRT, and we compare against MMLT implemented in the same system. Five scenes - Breakfast (1024×1024), Villa (1200×580), Bathroom (1280×720), Bidir (768 × 576), Living Room (1280 × 720) - with different geometry, lighting, and material configurations are rendered on a Mac pro with Intel Core i5 at 2.7GHz. Villa scene reference is rendered using MMLT in PBRT and the references of the other four scenes are rendered with BDPT in PBRT. Rendering each of those references costs several days. We set the maximum path length at 9 for Living Room scene and at 5 for the other four scenes.

Equal-time Comparison. We show the image comparison results in Figures 1 and 4. To make equal-time comparisons between MMLT and our method, we rendered all the five scenes. Because proposal failure paths are thought of as extra overheads in our method, the parameter of mutations per pixel should be set at a smaller value than in MMLT, as show in column "Mutations Per Pixel" of Table 3.

In order to obtain the statistic data of these comparisons, we define some counters in Algorithm 2: $TotalPaths$ is the total number of paths traced; $ExcludedPaths$ is the number of proposal failure paths excluded from the states of Markov chain; $FinalFailurePaths$ is the number of final failure paths after remedy; $AcceptancePaths$ is the number of paths accepted. All of these counters should be initialized to 0 before the beginning of rendering (line 5 of Algorithm 2). In the Algorithm 2, we add some other code for statistics: "$TotalPaths++$;" at line 6; "$ExcludedPaths++$;" at line 23; "$if(\alpha < 0.000001)FinalFailurePaths++$;" at line 28; "$AcceptancePaths++$;"

at line 31. We use the following equations to calculate *FailureRate* and *AcceptanceRate*.

$$FailureRate = \frac{FinalFailurePaths}{(TotalPaths - ExcludedPaths)}$$

$$AcceptanceRate = \frac{AcceptancePaths}{(TotalPaths - ExcludedPaths)}$$

These statistics are also recorded in Table 3.

Scenes	Algorithms	Mutations Per Pixel	Failure Rate	Acceptance Rate	RMSE
Breakfast	MMLT	150	37.37%	49.38%	0.082572
	Ours	100	0%	77.84%	0.069976
Villa	MMLT	200	62.82%	32.39%	0.083772
	Ours	80	0%	75.26%	0.070404
Bathroom	MMLT	280	40.00%	57.00%	0.120891
	Ours	150	0%	89.01%	0.103564
Bidir	MMLT	75	37.40%	57.82%	0.067776
	Ours	45	0%	90.18%	0.056806
Living Room	MMLT	670	51.12%	45.07%	0.129880
	Ours	200	0%	90.49%	0.102854

Table 3. Table of statistics of equal-time comparison (2 hours for Breakfast, 1.5 hours for Villa, 1 hour for Bathroom, 25 minutes for Bidir, and 110 minutes for Living Room). Because proposal failure paths are thought of as extra overheads in our method, the parameter of mutations per pixel should be set to a smaller value than in MMLT. We also show the comparisons of failure rate, acceptance rate and RMSE for these scenes. From the table, we can see that our method always produce better results (smaller RMSE) than MMLT does.

Breakfast Scene. Figure 1 shows an equal-time (2 hours) comparison on the Breakfast Scene which is illuminated by two lamps. Part of the scene, like the objects on the top of the desk, get direct illumination, however, the lighting for objects under the desk or over the lamps is much more complicated. From Figure 1 and table 3, we can see that MMLT shows suboptimal performance because about 37.37% of the paths that were used to reconstruct image carried no radiance. Giving special treatment to zero-contribution paths, our method reduces the percentage to around 1.54% and exhibits much better results with smaller RMSE. Our method distinguishes itself in those difficult settings where a large fraction of all of the possible proposal paths fail to carry any radiance in MMLT rendering, as shown in the three insets of Figure 1.

Villa Scene. The first part of Figure 4 shows an equal-time (1.5 hours) comparison on the Villa scene with complex materials and a difficult geometry configuration lit by outside environment daylight. This is a challenging scene because of the hard-to-find specular-diffuse-specular (SDS) light paths between the villa interior and the near-specular glass windows. The reference rendered by MMLT with 10000 mutations per pixel is still slightly noisy after several days of computation. Also, from Figure 4 and table 3, we can see that MMLT produces a lot of noises because more than 62.81% of the paths that were used to reconstruct image were zero-contribution. Our method considers zero-contribution proposal as failure and gives special treatment to it. As a result, the percentage was reduced to about 14.47 and higher quality image was obtained. If our method is used to render the image with the same RMSE of 0.083772 like MMLT does, more than 37% of the time will be saved.

Bathroom Scene. The second part of Figure 4 shows an equal-time (1 hour) comparison on the Bathroom scene which contains several different materials including diffuse, specular, and glossy. The scene is illuminated with a large area light source directly visible from the camera. Unlike the Villa scene, the major part of the scene is directly illuminated by the light source. Even in such a simple lighting situation, our method can still produce a better image than MMLT does in equal time. If our method is used to render the image with the same RMSE of 0.120981 like MMLT does, more than 45% of the time will be saved.

Bidir Scene. The third part of Figure 4 shows an equal-time (25 minutes) comparison on the Bidir scene. The illumination resembles the Breakfast scene whose part of objects get direct lighting and other parts not. If our method is used to render the image with the same RMSE of 0.067776 like MMLT does, about 28% of the time will be saved.

Living Room Scene. The last part of Figure 4 shows an equal-time (110 minutes) comparison on the Living Room scene. Light coming from outside environment enter the room through glass widows like the Villa scene does. Again, this kind of lighting makes rendering the scene a challenging task. What's more, the materials of the Living Room scene are more complex. The floor, the table and the paneling are made of substrate material, a layered model that varies between glossy specular and diffuse reflection depending on the viewing angle. The cups and the bottle on the table are glass. Other objects like the big mirror and the brushed stainless-steel lampshades also contribute to the complication of materials of the scene. All of this result that more than 51.12% of all paths that were used to reconstruct image in MMLT don't carry any radiance. Again, our method is even more efficient in rendering scenes with complex material and lighting. If our method is used to render the image with the same RMSE of 0.129880 like MMLT does, about 47% of the time will be saved.

MMLT	A	B	C	D	E	F
	20	40	85	170	340	670
Ours	O	P	Q	R	S	T
	10	20	35	75	150	310

Table 4. *Parameter settings of mutations per pixel for convergence comparison.* We used ABCDEF and OPQRST to label the resulting images rendered by MMLT and our method respectively as in Figure 5a.

Convergence Comparison. To make our method more convincing, we did a sequence of comparisons with different computations and compared the convergence of MMLT and our method. The mutations per pixel of the images rendered with similar time were set as Table 4. The resulting comparison images were shown in Figure 5a. Based on the comparison images and their error images in Figure 5a, we can see that our method converges much faster than MMLT does. We also calculated the RMSEs of each of these images and exhibited them in line chart as shown in Figure 5b. As the blue dash lines

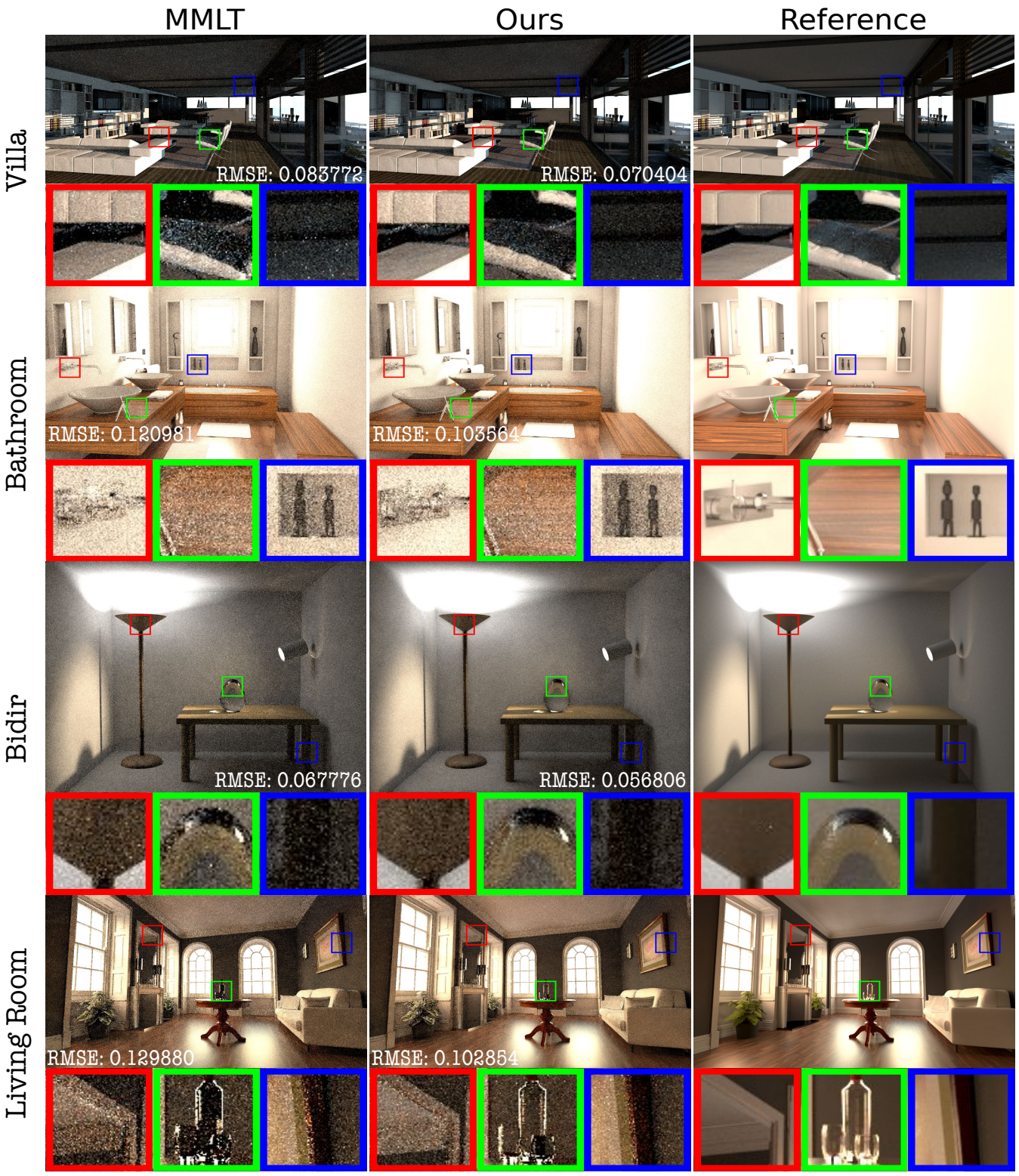

Fig. 4. *Equal-time comparisons.* These challenging scenes, Villa, Bathrooom, Bidir and Living Room, are of various complex material, lighting and geometry. RMSE is used as the indicator of image quality. Our method always produce better results, with smaller RMSE, than MMLT does.

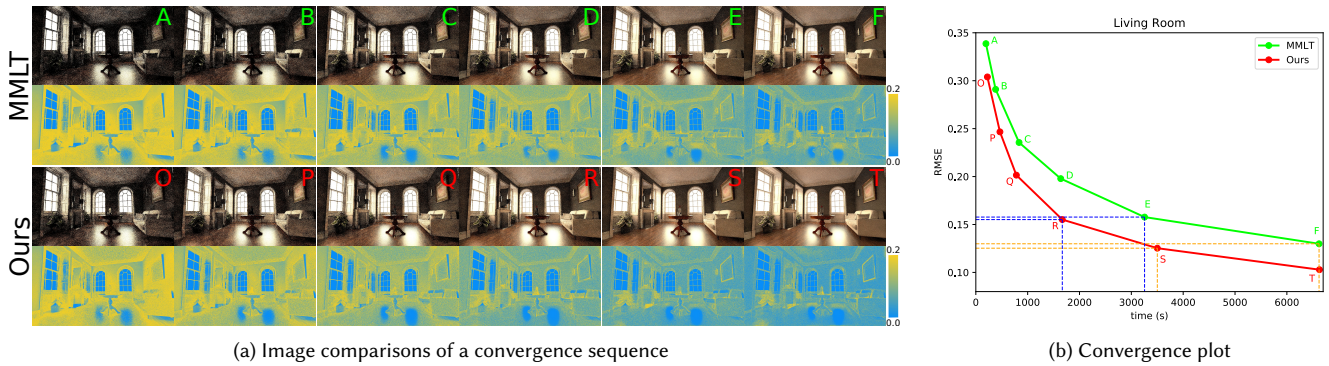

(a) Image comparisons of a convergence sequence

(b) Convergence plot

Fig. 5. *Convergence comparisons for the Living Room scene.* Based on the comparison images and their error images in (a), we can see that our method converges much faster than MMLT does. The RMSEs of each of these images are exhibited in line chart as (b). As the blue dash lines show, the RMSE of image R rendered with our method is slightly smaller than the RMSE of image E rendered with MMLT, but the rendering time of image R is just about half of image E. Also, as the orange dash lines show the comparison the RMSE of image S and image F, our method saves even bigger ratio of time.

mark in Figure 5b, the RMSE of image R rendered with our method is slightly smaller than the RMSE of image E rendered with MMLT, but the rendering time of image R is just about half of image E. Also, as the orange dash lines show the comparison the RMSE of image S and image F, our method saves even bigger ratio of time. Thus, the higher same-quality of images rendered by MMLT and our method, the bigger ratio of time will be saved by our method.

6.2 Extra Results

In order to further verify the effectiveness of our method and the fact that other MLT-type algorithms can be easily extended with our method, we now compare RJMLT [Bitterli et al. 2018] with our method. We extend both RJMLT and MMLT in Bitterli's original source code, Tungsten [Bitterli 2017], a renderer that is a much simpler and faster than PBRT, and get two new algorithms, RJMLT+PF and MMLT+PF ("PF" means Rectified Proposal Failure). Considering that the random seeds used in RJMLT are not fixed, the result of any single run of RJMLT may not be representative, so we use average behavior of many times of rendering with exactly same settings to do comparison test with other algorithms, which is why we do not include RJMLT in all of tests of the prior scenes as shown in Figure 4.

Here, we compare equal-time images of the Glass-Of-Water scene rendered with the four algorithms in Tungsten: MMLT, RJMLT, MMLT+PF, RJMLT+PF. We set the maximum path length at 15. Expected results should be: MMLT+PF is better than MMLT, and RJMLT+PF is better than RJMLT. First, we produce the two five-minute images of MMLT and MMLT+PF. (Five-minute images are of relatively high quality because of the fact that Tungsten is much simpler and faster than PBRT.) We find the parameters of RJMLT and RJMLT+PF to produce five-minute images, run RJMLT and RJMLT+PF with the parameters 50 times to produce 50 images respectively, and calculate the average RMSEs of RJMLT and RJMLT+PF with their own 50 images respectively. The Results are shown in Figure 6. For RJMLT and RJMLT+PF, while the two images are specially chosen from their own 50 images, which may not be representative, the RMSEs are the average of 50 results, which is reliable. In this scene, based on the RMSEs, we can see that: both RJMLT and MMLT+PF are better than MMLT; RJMLT+PF is the best (of course better than RJMLT); in particular, we get a bonus: *MMLT+PF is better than RJMLT*, which means that PF makes MMLT not just better than MMLT, but also better than RJMLT.

7 LIMITATIONS AND FUTURE WORK

As a MLT-type rendering algorithm, generally, our method is also only good at rendering challenging scenes which contain complex materials and lighting. Like other adaptive MLT-type algorithms, such as *MEMLT* [Jakob and Marschner 2012], *H^2MC* [Li et al. 2015], *HSLT* [Hanika et al. 2015] and *GeoMLT* [Otsu et al. 2018], extra computations are needed to address challenging parts of scenes. So, the number of mutations per pixel that can be finished in equal time as non-adaptive algorithms decreases, which may slightly affect the rendering of simple parts of the same scene. Our method cannot change/improve the original nature of the MLT-type algorithm that is extended with our method. For example, RJMLT+PF inherited the nature that the random seeds used are not fixed from RJMLT, which means that the result of any single run of RJMLT+PF may also not be representative, so average behavior of many times of rendering with exactly same settings must be used to show its effectiveness.

Providing remedies to minimize the impact of proposal failure without modifying mutation strategies is a new direction to improve the efficiency of MLT-type algorithms. We just presented a simple remedy in this paper, and we believe that many more efficient and sophisticated remedies can be developed to further decrease the serious impact caused by proposal failures in the future research. Considering that MCMC is widely used in various fields, the idea of remedy for proposal failures can be effectively introduced into these fields.

REFERENCES

Benedikt Bitterli. 2017. Tungsten Source Code. https://github.com/tunabrain/tungsten.

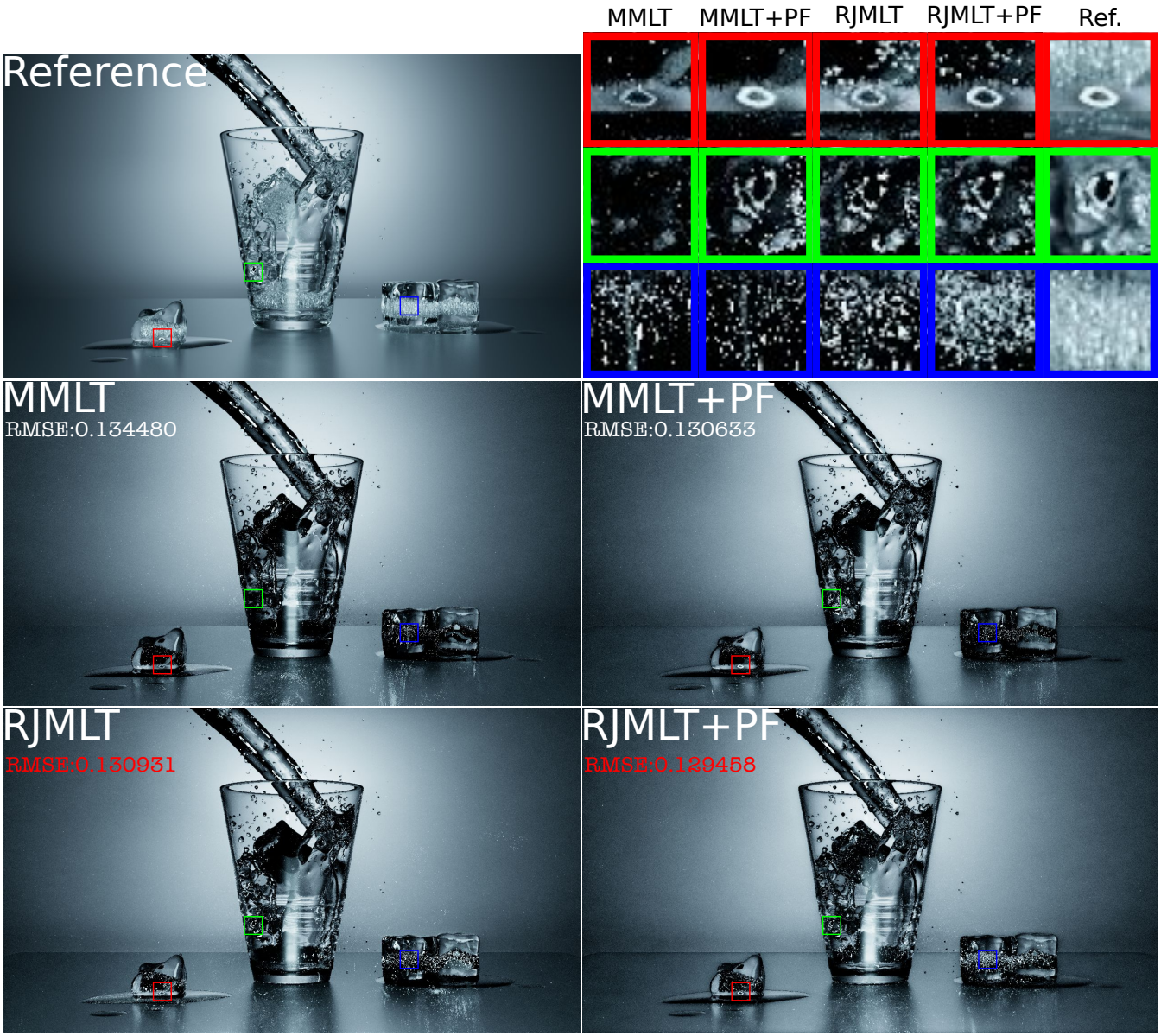

Fig. 6. *Equal-time comparisons with RJMLT.* "MMLT+PF" and "RJMLT+PF" are Rectified Proposal Failure extensions of MMLT and RJMLT respectively. Considering that the random seeds used in RJMLT are not fixed, the result of any single run of RJMLT may not be representative, so average behavior of many times of rendering with exactly same settings is used to do comparison test with other algorithms. For RJMLT and RJMLT+PF, while the two images are specially chosen from their own 50 images, which may not be representative, the RMSEs are the average of 50 results, which is reliable. In this scene, based on the RMSEs, we can see that: both RJMLT and MMLT+PF are better than MMLT; RJMLT+PF is the best (of course better than RJMLT); in particular, we get a bonus: *MMLT+PF is better than RJMLT*, which means that PF makes MMLT not just better than MMLT, but also better than RJMLT.

Benedikt Bitterli, Wenzel Jakob, Jan Novák, and Wojciech Jarosz. 2018. Reversible Jump Metropolis Light Transport using Inverse Mappings. *ACM Transactions on Graphics (Presented at SIGGRAPH)* 37, 1 (jan 2018). https://doi.org/10.1145/3132704

Adrien Gruson, Mickaël Ribardière, Martin Šik, Jiří Vorba, Rémi Cozot, Kadi Bouatouch, and Jaroslav Křivánek. 2017. A Spatial Target Function for Metropolis Photon Tracing. *ACM Trans. Graph.* 36, 1 (2017), 13. https://doi.org/10.1145/2963097

Toshiya Hachisuka and Henrik Wann Jensen. 2011. Robust Adaptive Photon Tracing using Photon Path Visibility. *ACM Trans. Graph* 30, 5 (2011). https://doi.org/10.1145/2019627.2019633

Toshiya Hachisuka, Anton S. Kaplanyan, and Carsten Dachsbacher. 2014. Multiplexed Metropolis Light Transport. *ACM Trans. Graph. (Proceedings of SIGGRAPH)* 33, 4 (July 2014), 10. https://doi.org/10.1145/2601097.2601138

Johannes Hanika, Anton Kaplanyan, and Carsten Dachsbacher. 2015. Improved half vector space light transport. *Computer Graphics Forum (Proc. EGSR)* 34, 4 (2015), 65–74.

W. K. Hastings. 1970. Monte Carlo sampling methods using Markov chains and their applications. *Biometrika* 57, 1 (1970), 97–109. https://doi.org/10.1093/biomet/57.1.97

Jared Hoberock and John C. Hart. 2010. Arbitrary Importance Functions for Metropolis Light Transport. *Computer Graphics Forum* (2010), 1993–2003. https://doi.org/10.1111/j.1467-8659.2010.01713.x

Wenzel Jakob and Stephen Marschner. 2012. Manifold exploration: a Markov chain Monte Carlo technique for rendering scenes with difficult specular transport. *ACM Trans. Graph. (Proc. SIGGRAPH)* 31, 4 (2012).

James T. Kajiya. 1986. The Rendering Equation. *In Computer Graphics (Proceedings of SIGGRAPH)* 20 (1986), 143–150. https://doi.org/10.1145/15922.15902

C. Kelemen, L. Szirmay-Kalos, G. ANTAL, and F. CSONKA. 2002. A simple and robust mutation strategy for the Metropolis light transport algorithm. *Computer Graphics Forum* 21, 3 (July 2002), 531–540.

Shinya Kitaoka, Yoshifumi Kitamura, and Fumio Kishino. 2009. Replica Exchange Light Transport. *Computer Graphics Forum* 28, 8 (2009), 2330–2342. https://doi.org/10.1111/j.1467-8659.2009.01540.x

Eric P. Lafortune and Yves D. Willems. 1993. Bi-Directional Path Tracing. *Proceedings of Compugraphics '93* (1993), 145–153.

Eric P. Lafortune and Yves D. Willems. 1996. Rendering Participating Media with Bidirectional Path Tracing. *Proceedings of the 7th Eurographics Workshop on Rendering* (1996), 91–100.

Tzu-Mao Li, Jaakko Lehtinen, Ravi Ramamoorthi, Wenzel Jakob, and Frédo Durand. 2015. Anisotropic Gaussian Mutations for Metropolis Light Transport Through Hessian-Hamiltonian Dynamics. *ACM Trans. Graph. (Proc. SIGGRAPH Asia)* 34, 6 (2015), 209:1–209:13.

N. Metropolis, N. Metropolis, M. N. Rosenbluth, A. H. Teller, and E. Teller. 1953. Equation of State Calculations by Fast Computing Machines. *J. Chem. Phys.* 21, 6 (1953), 1087–1092. https://doi.org/10.1063/1.1699114

Hisanari Otsu, Johannes Hanika, Toshiya Hachisuka, and Carsten Dachsbacher. 2018. Geometry-Aware Metropolis Light Transport. *ACM Transactions on Graphics (Proc. of SIGGRAPH Asia)* 37, 6, Article 278 (2018), 278:1–278:11 pages.

Hisanari Otsu, Anton S. Kaplanyan, Johannes Hanika, Carsten Dachsbacher, and Toshiya Hachisuka. 2017. Fusing State Spaces for Markov Chain Monte Carlo Rendering. *ACM Transactions on Graphics (Proc. of SIGGRAPH)* 36, 4, Article 74 (2017), 74:1–74:10 pages.

Jacopo Pantaleoni. 2017. Charted Metropolis Light Transport. *ACM Transactions on Graphics* 36 (2017).

Christian Robert. 2013. bounded target support. https://xianblog.wordpress.com/2013/07/08/bounded-target-support-2/#comments.

E. Veach. 1997. Robust Monte Carlo Methods for Light Transport Simulation. *PhD thesis, Stanford University* (1997).

Eric Veach and Leonidas J. Guibas. 1994. Metropolis Light Transport. *In Photorealistic Rendering Techniques (Proceedings of the Eurographics Workshop on Rendering)* (1994), 147–162. https://doi.org/10.1007/978-3-642-87825-1_11

Eric Veach and Leonidas J. Guibas. 1997. Metropolis Light Transport. *In Annual Conference Series on Computer Graphics (Proceedings of SIGGRAPH)* (1997), 65–76. https://doi.org/10.1145/258734.258775

Martin Šik, Hisanari Otsu, Toshiya Hachisuka, and Jaroslav Křivánek. 2016. Robust Light Transport Simulation via Metropolised Bidirectional Estimators. *ACM Transactions on Graphics (Proceedings of SIGGRAPH Asia)* 35, 6 (Nov. 2016), 12. https://doi.org/10.1145/2980179.2982411